Elsevier Editorial System(tm) for Computational Materials Science
Manuscript Draft

Manuscript Number:

Title: Ductility enhancement of layered stainless steel with nanograined interface layers

Article Type: Research Paper

Section/Category: Large Scale Systems

Keywords: Nanograined interface layer; Mechanical attrition treatment; Interface; Enhanced ductility; Cohesive finite element method

Corresponding Author: Ai Kah Soh,

Corresponding Author's Institution:

First Author: Xiang Guo

Order of Authors: Xiang Guo; G.J. Weng; Ai Kah Soh

Abstract: Combination of surface mechanical attrition treatment (SMAT) and co-rolling is a promising experimental methodology to design metals with high strength and high ductility. Recent results have revealed that brittle nanograined interface layer (NGIL) can enhance the ductility of the co-rolled SMATed stainless steel (SS). In the present study, the cohesive finite element method is used to show that the SS ductility is significantly enhanced with the increase of fracture toughness of coarse-grained layers and failure strain of NGIL. However the ductility will not increase if the NGIL thickness goes beyond 60 μm.

Suggested Reviewers: Shaohua Chen
chenshaohua72@hotmail.com
Professor Chen is an outstanding researcher in computational micromechanics.

Zishun Liu
liuzs@ihpc.a-star.edu.sg
Dr. Liu has great expertise in Computational Mechanics.

Qinghua Qin
qinghua.qin@anu.edu.au
An experienced researcher in Finite element method, boundary element method, Fracture and damage mechanics, Composite materials, Solid mechanics, Engineering computation.

# Ductility enhancement of layered stainless steel with nanograined interface layers

X. Guo[a,b], G.J. Weng[b,c], A.K. Soh[b,*]

[a] *Department of Mechanics, School of Mechanical Engineering, Tianjin University, Tianjin 300072, China; Tianjin Key Laboratory of Nonlinear Dynamics and Chaos Control, Tianjin 300072, China*

[b] *Department of Mechanical Engineering, The University of Hong Kong, Hong Kong*

[c] *Department of Mechanical and Aerospace Engineering, Rutgers University, New Brunswick, NJ 08903, USA*

**Abstract** Combination of surface mechanical attrition treatment (SMAT) and co-rolling is a promising experimental methodology to design metals with high strength and high ductility. Recent results have revealed that brittle nanograined interface layer (NGIL) can enhance the ductility of the co-rolled SMATed stainless steel (SS). In the present study, the cohesive finite element method is used to show that the SS ductility is significantly enhanced with the increase of fracture toughness of coarse-grained layers and failure strain of NGIL. However the ductility will not increase if the NGIL thickness goes beyond 60 μm.

*Keywords:* Nanograined interface layer; Mechanical attrition treatment; Interface; Enhanced ductility; Cohesive finite element method

---

* Corresponding author. Tel.: +852 28598061; fax: +852-28585415.

*E-mail address:* aksoh@hkucc.hku.hk (A.K. Soh).

## 1. Introduction

Among the newly-developed experimental approaches to design structural materials with both high strength and high ductility [1-7], one of the most promising techniques is believed to be a combination of surface mechanical attrition treatment (SMAT) and co-rolling, which can produce large-scale laminated nanostructured materials for structural applications [6,7]. Through SMAT, a nano-crystalline surface with 10-50 μm thickness can be generated for various metals to enhance their yield stress and fatigue life without altering their chemical compositions [8-11]. When such SMATed metals are placed on top of each other and then warm rolled, the process produces the co-rolled SMATed metals. This approach of combining SMAT with warm co-rolling has been successfully applied to generate laminated nanostructured 304 stainless steels (SS). The tensile experimental specimen of such SS with a length 20 mm and a width 1.8 mm in Refs. [6,7] is illustrated in Fig. 1a. Its yield stress has been found to reach 878 MPa and its failure strain 48%, which is three times that of the work-hardened steel with the same yield stress [6,7]. In the recent work by Guo et al. [12], the cohesive finite element method (CFEM) was employed to correlate the ductility of the co-rolled SMATed 304SS with the critical energy release rate of nanograined interface layer (NGIL). The simulation results showed that under external tensile load the brittle NGIL developed high density of microcracks, and this in turn toughened the co-rolled SMATed 304SS. This toughening mechanism was a direct reflection of the non-local cracking model suggested in [6,7]. In addition to the

energy release rate of NGIL, other factors could also affect the overall failure strain of the co-rolled SMATed 304SS. In this paper we will focus on how this important property is affected by

i) the failure strain of the NGIL,

ii) the fracture toughness, $K_{IC}$, of the coarse-grained layer (CGL), and

iii) the NGIL thickness.

It turns out that each of these parameters can have significant influence on the ductility of the material.

## 2. The cohesive finite element method

The cohesive finite element method (CFEM) and the eXtended finite element method (XFEM) have both proven to be effective tools in investigating the fracture process of structural materials. They produce similar crack speeds and crack paths, but at present the XFEM encounters some difficulties in modeling spontaneous multiple crack initiation, branching, and coalescence [13]. As most of the microcracks in NGILs are transverse cracks normal to the tensile direction [7,12] and our focus is on both nucleation and propagation of these multiple microcracks, not just on keeping track of a single crack, the CFEM is a more appealing approach. The CFEM allows the damage initiation/evolution and fracture processes to be modeled explicitly. It has been widely used to investigate both brittle and ductile fracture [14-18]. In the framework of CFEM, two approaches - intrinsic and extrinsic - are available when the

damage initiation site or the crack path is not known a priori. The intrinsic CFEM embeds the cohesive elements along boundaries of volumetric elements as part of the physical model [14], while the extrinsic CFEM, based on an extrinsic fracture initiation criterion, inserts the cohesive elements into the model as fracture develops [15]. The intrinsic CFEM has several advantages in model implementation and results interpretation [16]. This approach will be adopted in this investigation.

Many cohesive laws, which specify the constitutive relationships between interfacial traction and separation, have been developed for different conditions [17]. A bilinear cohesive law with two parameters, the cohesive strength $T_{\max}$ and the cohesive fracture energy $G_{\text{coh}}$, is widely used for its simplicity (Fig. 1b). Here $T_{\max}$ is the stress at which the damage initiates. The cohesive energy, $G_{\text{coh}}$, is the external energy supply required to create and fully break a unit surface area of the cohesive element; it is given by the area under the cohesive law, i.e., $G_{\text{coh}} = \int_0^{\delta_m^f} T(\delta)\,\mathrm{d}\delta = 0.5 T_{\max} \delta_m^f$, where $T$ is an effective traction, $\delta$ an effective separation, and $\delta_m^f$ the critical crack opening after which the traction becomes zero and the cohesive element totally fails. Near and inside the NGIL, the quadratic strain criterion for damage initiation and evolution is especially suitable to account for the multiaxial stress state and will be adopted for the entire specimen. From the view point of stiffness reduction, damage associated with the cohesive surface separation can also be defined in this context [19].

The co-rolled SMATed 304SS contains two phases, namely, the CGL with a

mean grain size of several microns and the NGIL with a mean grain size of about 50 nm. An analysis configuration with a length 1 mm and a width 0.9 mm is shown in Fig. 1c, and the fine structured FEM cross-triangular meshes with uniform size 10 by 10 μm is shown in Fig. 1d. Unless otherwise stated, the thickness of the NGIL is taken as 40 μm, the same as that in experimental investigation [6,7]. Constitutive parameters for the bulk and cohesive elements of the co-rolled SMATed 304SS are listed in Table 1. The isotropic, elasto-plastic constitutive relations are applied to both phases. The density, Young's modulus E, Poisson's ratio $\nu$, and flow stress for the two phases are the same as those in Ref. [12], where the flow stress of the CGL was measured directly and that of the NGIL was estimated from experimental results of the SMATed austenitic SS316L in Ref. [11]. The critical energy release rate of the CGL, $G_{\mathrm{Ic}}$, is obtained from $G_{\mathrm{Ic}} = K_{\mathrm{Ic}}^2\left(1-\nu^2\right)\Big/E$ in terms of its fracture toughness $K_{\mathrm{Ic}}$, which is taken as, unless otherwise stated, 100 $\mathrm{MPa}\sqrt{\mathrm{m}}$. The cohesive strength of the NGIL can be calibrated at different failure strain. To simulate the effects of cohesive strength and the critical energy release rate of the boundary between CGL and NGIL, two types of conditions are considered in CFEM calculations: i) a tough boundary which implies that its cohesive parameters are the same as those of the CGL, and ii) a brittle boundary which implies that its cohesive parameters are the same as those of the NGIL. These parameters are also listed in Table 1.

**Table 1.** Constitutive parameters for bulk and cohesive elements of co-rolled SMATed 304SS

| Compound | Density $(\mathrm{kg/m^3})$ | Yield stress | E $(\mathrm{GPa})$ | $\nu$ | $T_{\max}$ | $G_{\mathrm{coh}}$ |
|---|---|---|---|---|---|---|
| **Coarse-grained layer** | 8000 | $\sigma_0$ | 200 | 0.29 | $T_{\mathrm{m}}$ | $G_{\mathrm{Ic}}$ |
| **Nanograined interface layer** | 8000 | $\sigma_0^{'}$ | 200 | 0.29 | $T_{\mathrm{m}}^{'}$ | $G_{\mathrm{Ic}}^{'}$ |
| **Tough boundary** | ... | … | … | … | $T_{\mathrm{m}}$ | $G_{\mathrm{Ic}}$ |
| **Strong boundary** | ... | … | … | … | $T_{\mathrm{m}}^{'}$ | $G_{\mathrm{Ic}}^{'}$ |

## 3. Results and discussion

Within the above-developed framework, we have investigated the effects of (i) the failure strain of the NGIL, (ii) the fracture toughness of the CGL, and (iii) the thickness of the NGIL on the overall failure strain of the co-rolled SMATed 304SS.

In applying CFEM to ductile materials, plastic deformation and damage process tend to compete with each other so that the failure strain of the material is a natural outcome of the combined effects of bulk constituent response, interfacial behavior, and applied load. Therefore, the cohesive strength can be calibrated by comparing the simulation with experimental results. It has been confirmed that the failure strain is sensitive to the ratio of the cohesive strength to the yield stress of ductile materials [12,18]. The failure strain of the NGIL in [6,7] has been estimated to be about 3.26% [12], about the same value for the nanocrystalline 316L austenitic SS [11]. Its effect on the overall failure strain of the co-rolled SMATed 304SS is now of interest. Here

the critical energy release rate of the NGIL is taken as 60 $Jm^{-2}$ [12]. The cohesive strength of the NGIL, $T_m^{'}$ (a prime indicates that the quantity is associated with the NGIL while unprimed values refer to the CGL), is calibrated as 1.89 GPa, which represents 1.479 times of its yield stress $\sigma_0^{'}$ when its failure strain is 3.26%, as illustrated in Fig. 2. Similarly, the cohesive strength of the NGIL is calibrated as 1.75 GPa, which represents 1.369 times of its yield stress $\sigma_0^{'}$, when its failure strain is 2.5%. This implies that when the critical energy release rate is fixed, the cohesive strength increases with the failure strain.

With the calibrated cohesive strength of the NGIL, simulations are carried out at two levels of CGL cohesive strength ($T_m$ =1.87$\sigma_0$ and 1.94$\sigma_0$ with $\sigma_0$ its yield stress) and for two types of boundaries (tough and strong boundaries). Figs. 3a-b shows the simulated stress-strain curves for the co-rolled SMATed 304SS when the failure strains of NGIL are 2.5% and 3.26%, respectively. The experimental result in Ref. [7] is also plotted alongside for comparison. The scattered nature of the curves indicates that both the cohesive strength level of the CGL and the boundary type play significant role in the deformation process. The smallest overall failure strain in each figure is always associated with the case of smaller CGL cohesive strength (1.87$\sigma_0$). More importantly, it is observed that, when the failure strain of the NGIL increases from 2.5% to 3.26%, the largest overall failure strain of the specimen can increase from 45% to 51%, gaining significant ductility.

In this laminated system the CGL effectively serves as the substrate for the NGIL,

so an investigation on the effect of its fracture toughness on the overall failure strain can provide insights into whether the combination of SMAT and co-rolling can toughen other types of SS as well. We used the same parameters as those in Fig. 3b, but with two different values of $K_{\mathrm{Ic}}$ for CGL, 80 and 120 $\mathrm{MPa}\sqrt{\mathrm{m}}$, to investigate. The results are shown in Fig. 4a and b, respectively. It can be seen from Figs. 4a and 3b that all four overall failure strains increases substantially as $K_{\mathrm{Ic}}$ increases from 80 to 100 $\mathrm{MPa}\sqrt{\mathrm{m}}$. It can be found in Figs. 3b and 4b that the largest overall failure strain has minor increase as $K_{\mathrm{Ic}}$ changes from 100 to 120 $\mathrm{MPa}\sqrt{\mathrm{m}}$ while all four overall failure strains reach a level of 44-52%.

The dependence of the overall failure strain on the thickness of the NGIL deserves careful investigation because extensive trials on different NGIL thickness will cost tremendous experimental efforts in SMAT and co-rolling processes. To uncover this effect, we use the same NGIL cohesive strength as those in Figs. 3a and b, but this time with the NGIL thickness 60 μm. The corresponding results are shown in Fig. 5a and b, respectively, with the same NGIL failure strains, 2.5% and 3.26%. A direct comparison between Figs. 5a-b and Figs. 3a-b shows that the ductility of the co-rolled SMATed 304SS has significantly decreased at this large NGIL thickness. At an even larger thickness, 80 μm, the largest overall failure strain is found to remain relatively unchanged, but the smallest overall failure strain (the shortest curve) actually decreases from 26% to 20%. One is led to conclude that, even though introduction of the NGIL is beneficial to the overall ductility of the co-rolled SMATed

SS, a too-large thickness can become detrimental.

A closer look at Fig. 5 further indicates that the cohesive strength level of the CGL has a larger influence on the overall failure strain than the boundary type. This is evident from the fact that the one with the slightly larger cohesive strength ($1.94\sigma_0$) has larger overall failure strain than the one with the smaller cohesive strength ($1.87\sigma_0$). In addition, we could also see from Figs. 5a-b that, with the change of failure strain of the NGIL from 2.5% to 3.26% and $T_{\mathrm{m}}^{'}$ from $1.369\sigma_0^{'}$ to $1.479\sigma_0^{'}$, the strain level at which incipient damage initiates increases from less than 4% to around 6%, and the associated stress drop in the stress-strain curves also becomes more pronounced.

The change of the overall ductility is closely associated with the damage process of NGIL. To explore this issue further, we check the deformation process and concentrate on the nucleation and propagation of multiple microcracks in this layer. Figs. 6a-c illustrate the damage distribution in the co-rolled SMATed 304SS with the overall strain 0.12 for the cases of larger cohesive strength ($1.94\sigma_0$) and tough boundary, with the NGIL thickness 40, 60, and 80 μm, respectively. For better illustration, horizontal dashed lines are used to indicate the location of the deformed NGILs. Due to the intrinsically brittle nature of the NGIL, it can be seen from Fig. 6 that the size of damaged zones, i.e., the length of transverse microcracks, is relatively easy to reach the level of the NGIL thickness. As a result, the SS with thick NGILs will have longer microcracks, compared with the SS with thin NGILs. This explains

the observed substantial decrease in the ductility of the SS when the NGIL thickness increases from 40 to 60 μm. In addition to the requirement that microcracks must be sufficiently dense as proposed in Guo et al. [12], these simulations indicate that microcrack features have to be tiny in order to be effective to enhance the ductility of the SS.

The co-rolled SMATed 304SS specimens in above simulations are without any pre-crack. We have also conducted some simulations of the co-rolled SMATed 304SS specimen with a pre-crack, which is 10 μm long and located in center of the NGIL. We use the same NGIL cohesive strength as those in Figs. 3b (and also 5b), where $T_{\mathrm{m}}^{'}$ is $1.479\sigma_0^{'}$ when its failure strain is 3.26%. Figs. 7a-c show the corresponding simulated stress-strain curves for the co-rolled SMATed 304SS pre-cracked specimen, with the NGIL thickness 40, 60 and 80 μm, respectively. It can be found that the largest overall failure strain decreases markedly from 32% in Fig. 7a to 24% in Fig. 7b when the NGIL thickness increases from 40 to 60 μm, and further decreases to 8% in Fig. 7c with the NGIL thickness 80 μm. Although the pre-crack in the NGIL has the same initial length, its length can reach the level of the NGIL thickness, that is, the pre-crack can penetrate the entire NGIL easily. Therefore, a pre-crack is more detrimental in the thick NGIL than in the thin one. In this indirect way we have also confirmed our above finding that the overall failure strain can decrease substantially if the NGIL thickness increases beyond certain limit.

## 4. Conclusions

In this study we have employed an intrinsic CFEM framework, which has the capability of resolving the initiation and evolution of multiple microcracks, to study the influence of multiple factors on the overall failure strain of the co-rolled SMATed 304SS. It is found that the cohesive strength level of the CGL has a larger influence on the overall failure strain than the type of interface boundary. When the critical energy release rate of the NGIL is constant, the ductility of the SS can be enhanced with increased NGIL failure strain and CGL fracture toughness. On the other hand, thick NGIL is found to be detrimental to the SS ductility. Thus to enhance the SS ductility, the microcracks not only need to be sufficiently dense but also adequately small, and this requires comparatively thinner NGILs. Since comprehensive experimental investigations on these multiple factors are expensive to carry out and thus not particularly feasible, this systematic simulation could provide significant insights into the complex nature of the deformation process until failure. The obtained results can also serve as a guideline for future experimental investigations on SMAT and the co-rolling technique.

## Acknowledgements

Support from the Research Grants Council of the Hong Kong Special Administrative Region (Project no. CityU8/CRF/08) is gratefully acknowledged. X. Guo also acknowledges the support from National Natural Science Foundation of

China (Project No. 11102128), and G.J. Weng thanks the support of the HKU Visiting Research Professor Scheme 2010-2013.

## References

[1] R.Z. Valiev, I.V. Alexandrov, Y.T. Zhu, T.C. Lowe, J. Mater. Res. 17 (2002) 5-8.

[2] Y.H. Zhao, J.F. Bingert, X.Z. Liao, B.Z. Cui, K. Han, A.V. Sergueeva, et al., Adv. Mater. 18, (2006) 2949-2953.

[3] C.C. Koch, Scripta Mater. 49 (2003) 657-662.

[4] Y.H. Zhao, X.Z. Liao, S. Cheng, E. Ma, Y.T. Zhu, Adv. Mater. 18 (2006) 2280-2283.

[5] Y.M. Wang, M.W. Chen, F.H. Zhou, E. Ma, Nature 419 (2002) 912-915.

[6] A.Y. Chen, J.B. Zhang, J. Lu, W. Lun, H.W. Song, Mater. Lett. 61 (2007) 5191-5193.

[7] A.Y. Chen, D.F. Li, J.B. Zhang, H.W. Song, J. Lu, Scripta Mater. 59 (2008) 579-582.

[8] N.R. Tao, Z.B. Wang, W.P. Tong, M.L. Sui, J. Lu, K. Lu, Acta Mater. 50 (2002) 4603-4616.

[9] H.W. Zhang, Z.K. Hei, G. Liu, J. Lu, K. Lu, Acta Mater. 51 (2003) 1871-1881.

[10] T. Roland, D. Retraint, K. Lu, J. Lu, Scripta Mater. 54 (2006) 1949-1954.

[11] X.H. Chen, J. Lu, L. Lu, K. Lu, Scripta Mater. 52 (2005) 1039-1044.

[12] X. Guo, A.Y.T. Leung, A.Y. Chen, H.H. Ruan, J. Lu, Scripta Mater. 63 (2010)

403-406.

[13] J.H. Song, H. Wang, T. Belytschko, Comput. Mech. 42 (2008) 239-250.

[14] A. Needleman, ASME J. Appl. Mech. 54 (1987) 525-531.

[15] G.T. Camacho, M. Ortiz, Int. J. Solids Struct. 33 (1996) 2899-2938.

[16] Z. Zhang, G.H. Paulino, W. Celes, Int. J. Numer. Methods Eng. 72 (2007) 893-923.

[17] N. Chandra, H. Li, C. Shet, H. Ghonem, Int. J. Solids Struct. 39 (2002) 2827-2855.

[18] A. Cornec, I. Scheider, K.H. Schwalbe, Eng. Fract. Mech. 70 (2003) 1963-1987.

[19] ABAQUS, ABAQUS theory manual and user's manual, version 6.8, Dassault (2011).

## Captions:

**Fig. 1.** (color online) (a) (not to scale) Experimental specimen with a length 20 mm and a width 1.8 mm in Refs. [6,7], (b) a bilinear cohesive law, (c) analysis configuration with a length 1 mm and a width 0.9 mm, and (d) cross-triangular meshes with uniform size 10 by 10 $\mu$m.

**Fig. 2.** (color online) Calibrated cohesive strength of the NGIL with energy release rate 60 $Jm^{-2}$ and tensile failure strain 3.26%.

**Fig. 3.** (color online) Effects of failure strain of NGIL on the overall ductility. It is (a) 2.5% and (b) 3.26% ((b) taken from [12]). Calculation was made with NGIL thickness 40 μm as in experiment.

**Fig. 4.** (color online) Effects of fracture toughness of CGL on the overall ductility. $K_{IC}$ is (a) 80 $MPa\sqrt{m}$ and (b) 120 $MPa\sqrt{m}$. These two figures are to be compared with the figure in Fig. 3b where $K_{IC}$ is 100 $MPa\sqrt{m}$.

**Fig. 5.** (color online) Simulated stress-strain curves for the co-rolled SMATed 304SS at NGIL thickness 60 μm, with failure strains in (a) 2.5% and in (b) 3.26%. These two figures are to be compared with those in Figs. 3a and b, to see that this larger NGIL thickness leads to a lower overall failure strain. Note that the experimental curve [7] is

associated with the specimen with NGIL of 40 μm thickness.

**Fig. 6** (color online) Damage distribution in the co-rolled SMATed 304SS with the overall strain 0.12 for the case of larger cohesive strength ($1.94\sigma_0$) and tough boundary with the NGIL thickness (a) 40, (b) 60, and (c) 80 μm.

**Fig. 7.** (color online) Effects of the NGIL thickness on the overall ductility of a pre-cracked specimen. The thicknesses are 40, 60, and 80 μm in (a), (b), and (c), respectively.

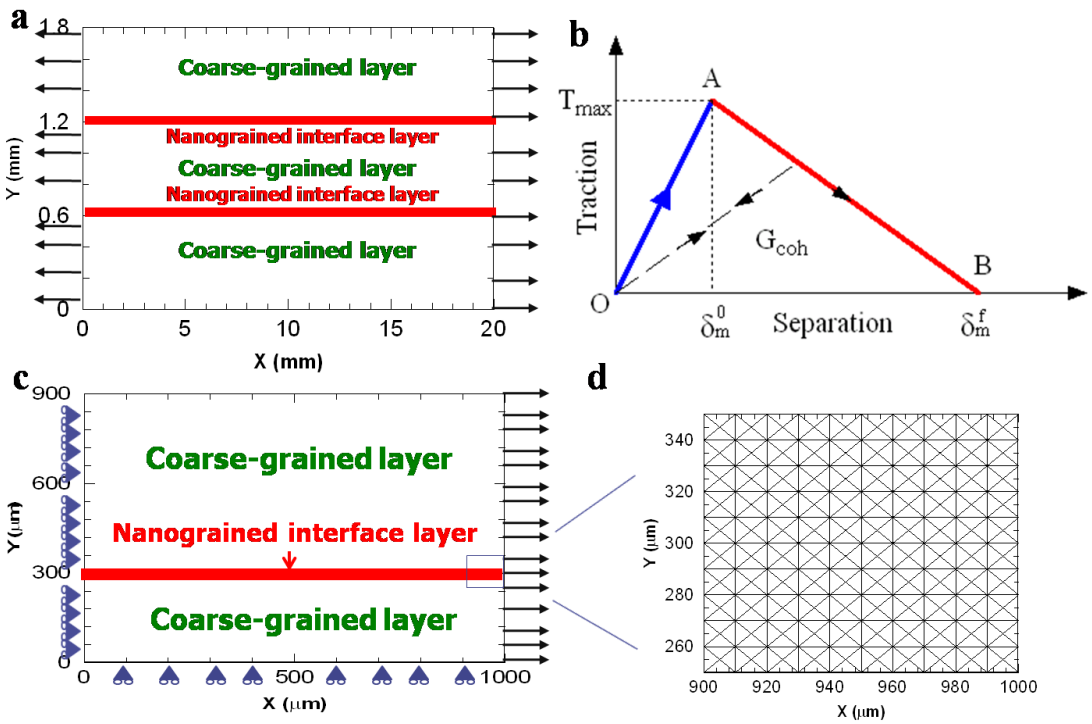
a
1.8
1.2
0.6
0
Y (mm)
Coarse-grained layer
Nanograined interface layer
Coarse-grained layer
Nanograined interface layer
Coarse-grained layer
0
5
10
15
20
X (mm)
b
A
$T_{max}$
Traction
$G_{coh}$
B
O
$\delta_m^0$
Separation
$\delta_m^f$
c
900
600
300
0
Y (μm)
Coarse-grained layer
Nanograined interface layer
Coarse-grained layer
0
500
1000
X (μm)
d
340
320
300
280
260
Y (μm)
900
920
940
960
980
1000
X (μm)

**Fig. 1**

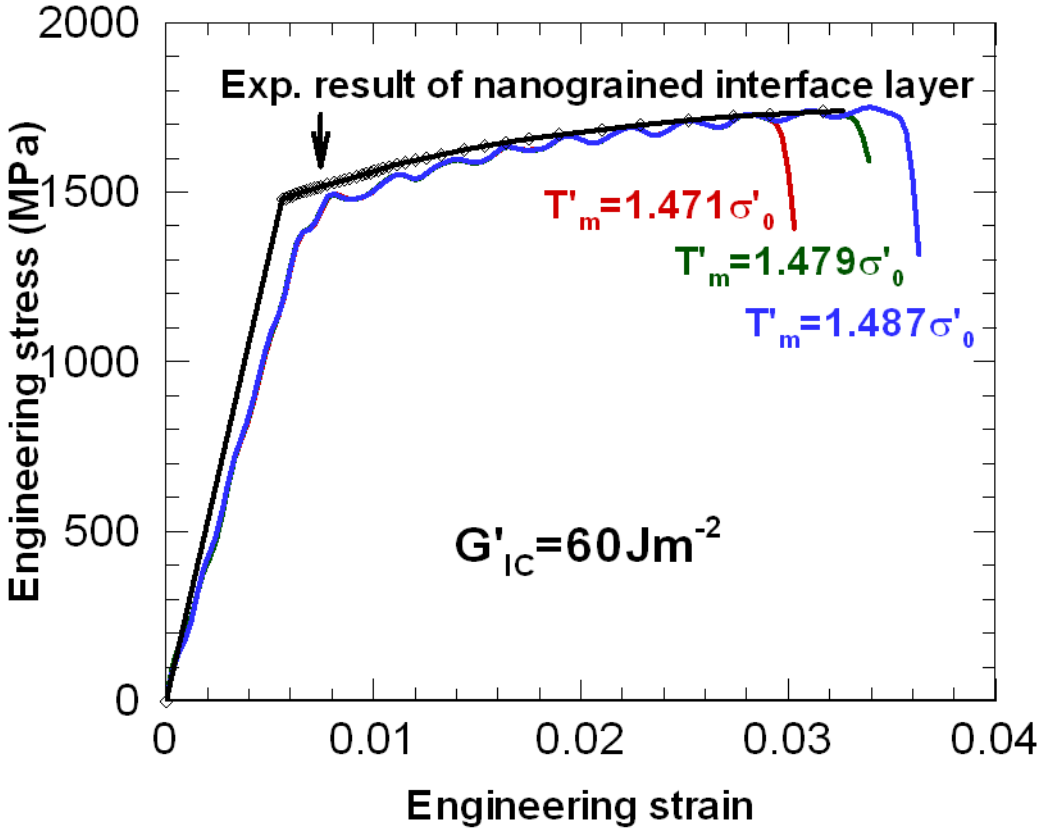
Exp. result of nanograined interface layer
T'm=1.471σ'0
T'm=1.479σ'0
T'm=1.487σ'0
G'IC=60Jm-2
Engineering stress (MPa)
Engineering strain
2000
1500
1000
500
0
0
0.01
0.02
0.03
0.04

**Fig. 2**

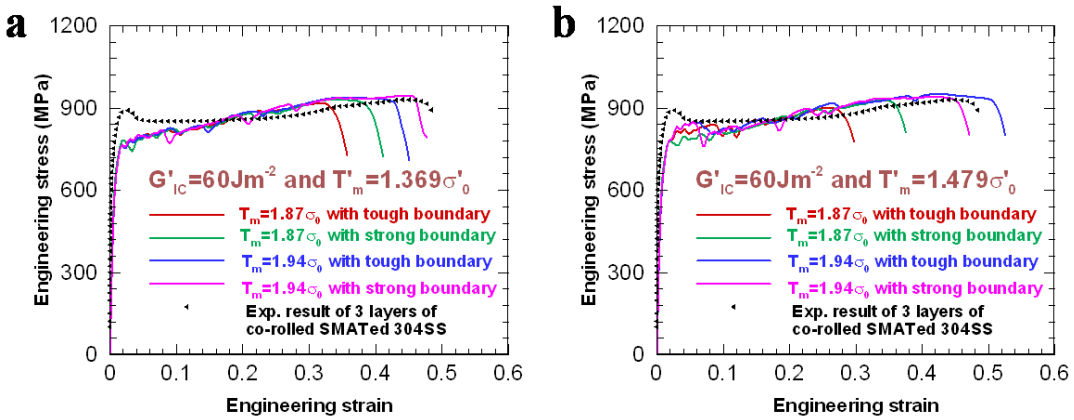
a
b
Engineering stress (MPa)
Engineering strain
G'IC=60Jm-2 and T'm=1.369σ'0
G'IC=60Jm-2 and T'm=1.479σ'0
Tm=1.87σ0 with tough boundary
Tm=1.87σ0 with strong boundary
Tm=1.94σ0 with tough boundary
Tm=1.94σ0 with strong boundary
Exp. result of 3 layers of co-rolled SMATed 304SS

**Fig. 3**

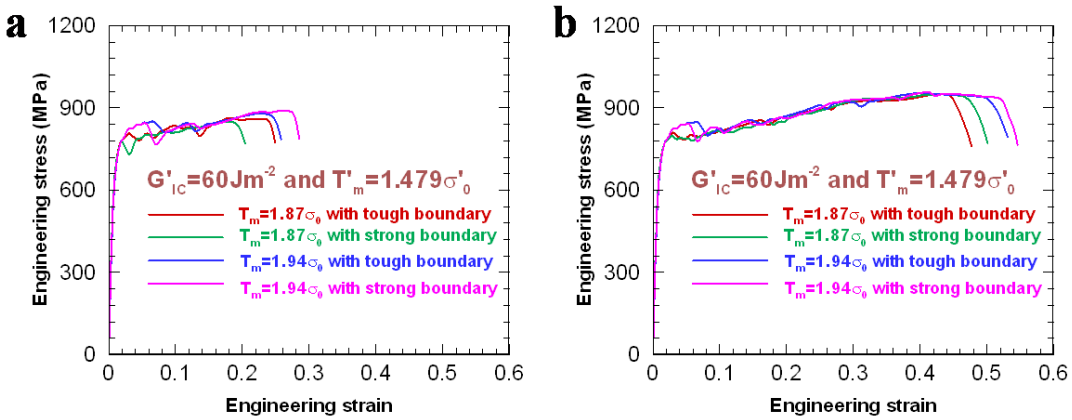
a
b
Engineering stress (MPa)
Engineering strain
G'IC=60Jm-2 and T'm=1.479σ'0
Tm=1.87σ0 with tough boundary
Tm=1.87σ0 with strong boundary
Tm=1.94σ0 with tough boundary
Tm=1.94σ0 with strong boundary

**Fig. 4**

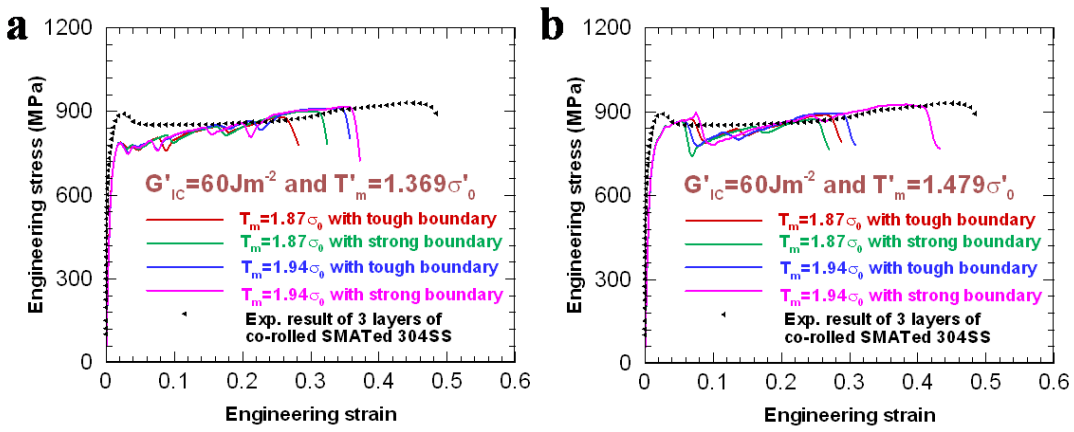
a
b
Engineering stress (MPa)
Engineering strain
G'IC=60Jm-2 and T'm=1.369σ'0
G'IC=60Jm-2 and T'm=1.479σ'0
Tm=1.87σ0 with tough boundary
Tm=1.87σ0 with strong boundary
Tm=1.94σ0 with tough boundary
Tm=1.94σ0 with strong boundary
Exp. result of 3 layers of co-rolled SMATed 304SS

**Fig. 5**

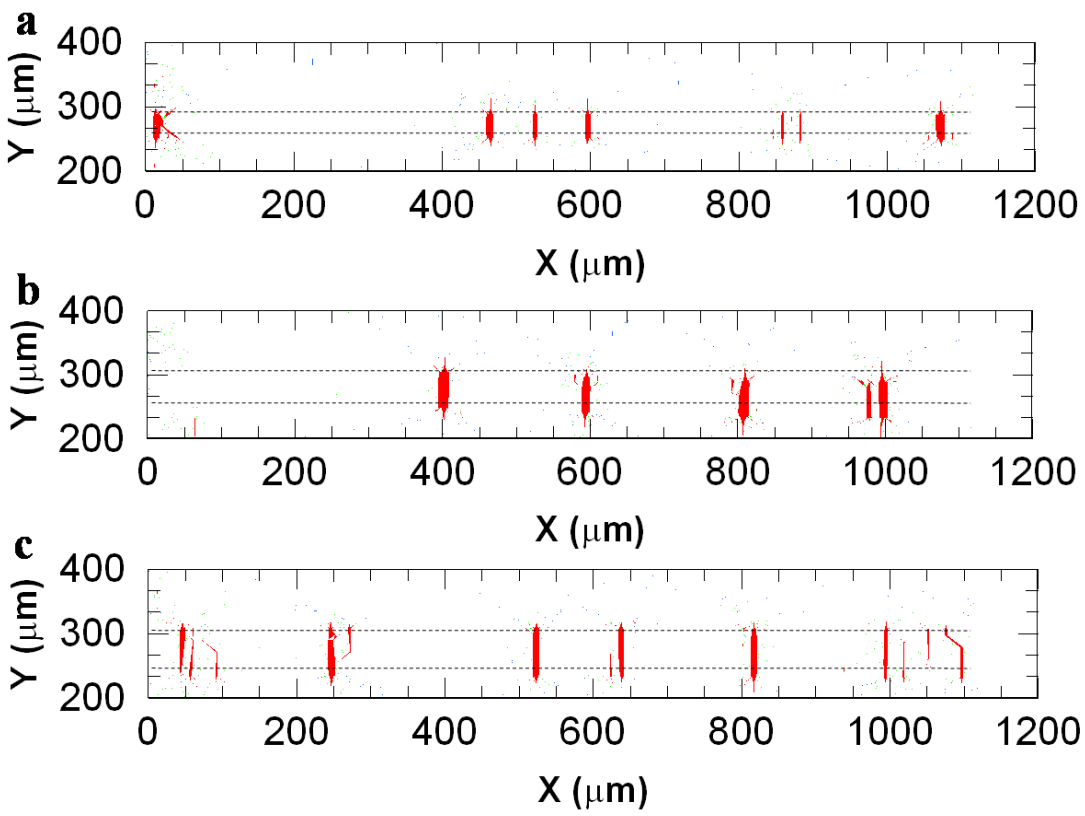


**Fig. 6**

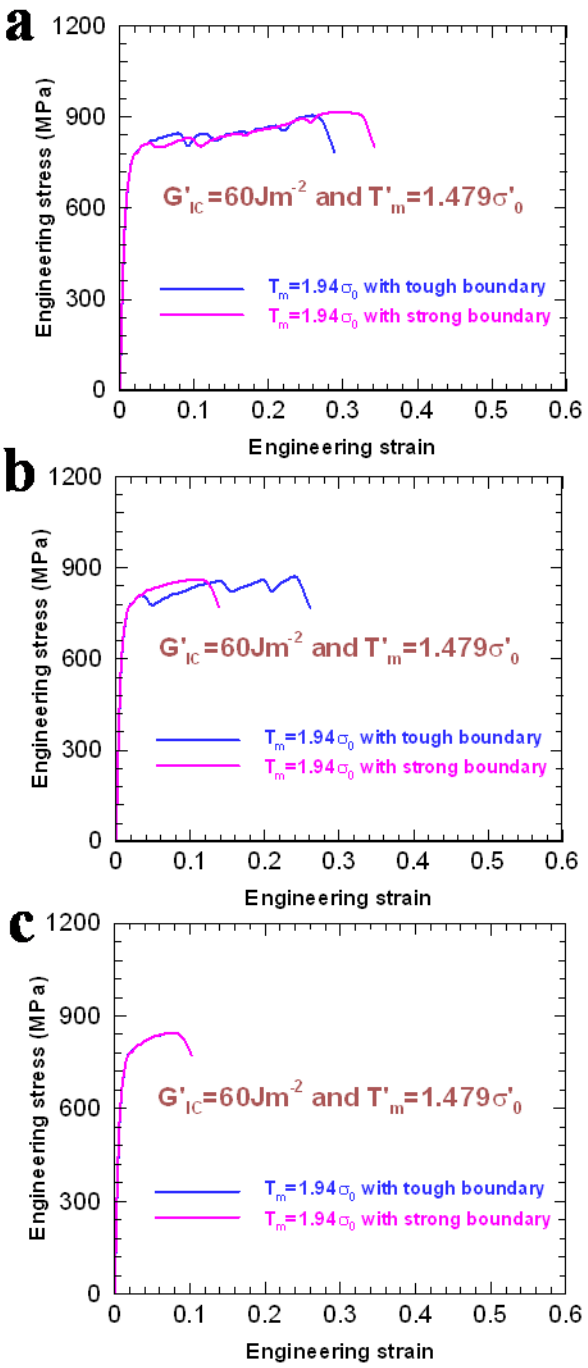
a
b
c
Engineering stress (MPa)
Engineering strain
0
300
600
900
1200
0.1
0.2
0.3
0.4
0.5
0.6
G'IC=60Jm-2 and T'm=1.479σ'0
Tm=1.94σ0 with tough boundary
Tm=1.94σ0 with strong boundary

**Fig. 7**